

Reconfigurable Intelligent Surfaces-Enabled Vehicular Networks: A Physical Layer Security Perspective

Abubakar Makarfi, *Member, IEEE*, Khaled M. Rabie, *Member, IEEE*, Omprakash Kaiwartya, *Member, IEEE*, Kabita Adhikari, *Member, IEEE*, Xingwang Li, *Senior Member, IEEE*, Marcela Quiroz-Castellanos, Rupak Kharel, *Senior Member, IEEE*.

Abstract—This paper studies the physical layer security (PLS) of a vehicular network employing reconfigurable intelligent surfaces (RISs). RIS technologies are emerging as an important paradigm for the realisation of next-generation smart radio environments, where large numbers of small, low-cost and passive elements, reflect the incident signal with an adjustable phase shift without requiring a dedicated energy source. Inspired by the promising potential of RIS-based transmission, we investigate the PLS of two vehicular network system models: One with vehicle-to-vehicle communication with the source employing a RIS-based access point, and the other is in the form of a vehicular adhoc network (VANET), with a RIS-based relay deployed on a building; both models assume the presence of an eavesdropper. The performance of the proposed systems are evaluated in terms of the average secrecy capacity (ASC) and the secrecy outage probability (SOP). We present accurate analytical expressions for the two performance metrics and study the impact of various system parameters on the overall performance of the two considered system configurations. Monte-Carlo simulations are provided throughout to validate the results. The results show that performance of the system in terms of the ASC and SOP is affected by the location of the RIS-relay as well as the number of RIS cells. Moreover, upto an order magnitude gain could be achieved within certain regions when the number of RIS cells are doubled, clearly indicating the benefit of employing a RIS configuration.

Index Terms—Beyond 5G, physical layer security, reconfigurable intelligent surfaces, secrecy capacity, secrecy outage probability, vehicular communications, vehicular networks.

I. INTRODUCTION

Reconfigurable intelligent surfaces (RISs), otherwise known as Large Intelligent Surfaces, Intelligent Reflecting Surfaces, reflector-arrays or intelligent walls, have recently gained much research attention for beyond 5G technology applications. This emerging communication paradigm is considered a potential

enabling technology in realising the concept of “smart radio environments” employed at the physical layer to control the propagation environment in order to improve signal quality and coverage [1], [2]. RISs are man-made surfaces of electromagnetic material (known as a metasurface) that are electronically controlled with integrated electronics and have unique wireless communication capabilities [3]. These man-made surfaces are composed of arrays of passive scattering elements with specially designed physical structures, where each scattering element can be controlled in a software-defined manner to change the phase shift and other signal characteristics, of the incident signals on the scattering elements [4]. The possibility of controlling the reflective interface converts the traditional random radio environment into a smart space to support several applications beneficial to wireless communications [3], [5], [6].

RIS-based transmission concepts have been shown to be completely different from existing multiple-input multiple-output (MIMO), beamforming and amplify-and-forward/decode-and-forward relaying paradigms. The large number of small, low-cost and passive elements on a RIS, only reflect the incident signal with an adjustable phase shift without requiring a dedicated energy source for RF processing or retransmission [7], which is particularly beneficial for its energy efficiency feature. Key benefits of the RIS-enabled communication in beyond 5G applications have been investigated with respect to the propagation channel [8]–[10], energy efficiency [11], [12], signal-to-noise ratio (SNR) maximisation [7], improving signal coverage [13], improving massive MIMO systems [14]–[16], improved interference suppression capability [17], [18], beamforming optimisation [19]–[22] and multi-user networks [11], [23], [24], for enhanced capacity, spectral efficiency and higher rates. Benefits have also been demonstrated for RIS-assisted physical layer security (PLS) [25]–[29] purposes, due to the flexibility of simultaneously enhancing or suppressing signal beams to different users [4]. It is worth noting that, PLS is achieved by employing the inherent characteristics of the propagation channels, such as interference, fading and noise to realise keyless secure transmission through signal processing approaches.

With regards to PLS in vehicular communications, the rapid advancements towards autonomous vehicles and smart/cognitive transportation networks, have made the secu-

A. U. Makarfi and R. Kharel are with the Department of Computing and Mathematics, Manchester Metropolitan University, Manchester, UK, M15 6BH (e-mails: {a.makarfi; r.kharel}@mmu.ac.uk).

K. M. Rabie is with the Department of Engineering, Manchester Metropolitan University, Manchester, UK, M15 6BH (e-mail: k.rabie@mmu.ac.uk).

O. Kaiwartya is with the School of Science and Technology, Nottingham Trent University, UK (e-mail: omprakash.kaiwartya@ntu.ac.uk).

K. Adhikari is with the School of Engineering, Newcastle University, Newcastle, UK, NE1 7RU (email: kabita.adhikari@ncl.ac.uk).

X. Li is with the School of Physics and Electronic Information Engineering, Henan Polytechnic University, Jiaozuo, China (e-mail: lixingwang@hpu.edu.cn).

M. Quiroz-Castellanos is with the Artificial Intelligence Research Center, Universidad Veracruzana, Mexico (e-mail: maquiroz@uv.mx).

urity of vehicular networks become even more important in order to ensure safety and minimise the risk of abuse or attacks [30]–[33]. Although several researchers have studied PLS in vehicular networks without the use of RISs [34]–[38], or non-vehicular RIS-assisted PLS for wireless applications [4], none of these works studied PLS of RIS-enabled vehicular networks as well as PLS of such networks.

Inspired by the promising potential of RIS-based transmission for both PLS and vehicular network communication, as well as the importance of security to vehicular networks, this paper is therefore dedicated to studying the PLS of two vehicular network models. We first consider a vehicle-to-vehicle (V2V) network with the source employing a RIS-based access point (for transmission), and in the second model we consider a vehicular adhoc network (VANET), with a RIS-based relay deployed on a building. Both models assume the presence of an eavesdropper. The performance of the proposed systems are evaluated in terms of the average secrecy capacity (ASC) and the secrecy outage probability (SOP).

There is a four-fold motivation for this research. Firstly, RIS-based technologies can be targeted for mobile nodes in vehicular networks due to the ease of deployability and flexible configuration that allows for deployment in several shapes, locations and sizes, from tens to hundreds of cells [3]. Secondly, existing RIS related literature have shown that most RIS-enabled applications are designed with the RIS as a reflector [3], [4], since the key benefit of employing a RIS is to control the radio environment for transmissions through smart reflections. However, other studies have adopted the RIS as a transmitter (or access point) [3], [7] or RIS as a signal receiver [39]. In this research, we consider two models adopting the RIS as a reflector and as a transmitter as applicable to vehicular networks. Thirdly, the mobility effect of nodes have been shown to impact the performance of vehicular nodes (see for e.g., [40]), although several previous studies assume quasi-static node positions due to ease of analysis. It has however been shown recently, that rapid fluctuations in the received signal strength due to the doppler effect can be effectively reduced by using the real-time tuneable RISs¹ [41]. Fourthly, the need for accurate analytical analysis for easily determining PLS parameters given that the existing literature on RIS-assisted PLS for non-vehicular applications have only reported some initial simulation results [4].

From the aforementioned, this study therefore presents the following contributions:

- We present a novel analysis of possible implementation of RIS to vehicular networks. To the best of the authors' knowledge, this is the first analysis of RIS-enabled vehicular networks, as well as the first time study of the PLS of such networks.
- We study the PLS of two possible vehicular network models. The first model considers a V2V network with the source vehicle employing a RIS-based access point (AP) for transmission. In the second model, we consider

a VANET with a source station transmission via a RIS-based relay. Such a RIS-relay could be deployed on a building as part of a smart infrastructure within a smart city environment.

- The PLS analysis is achieved by analyzing and deriving expressions for the ASC and the SOP of the system. The derived expressions allow for the ease of investigation of key system parameters.
- For the ASC, accurate closed-form approximations are further presented to make the analysis of key parameters more tractable. On comparison with the exact derived expressions, it will be observed that these approximations are highly accurate within the regions of interest. Moreover, with the approximate expressions, it becomes easier to gain insights into the behavior of the considered scenarios.
- The distances of the legitimate and eavesdropper nodes are taken into account along with realistic fading scenarios considered for the base stations and the vehicular mobile nodes.

For all the scenarios considered in this work, Monte Carlo simulations are provided to verify the accuracy of the analysis. The results show that the performance of the system in terms of the secrecy capacity is improved with the use of the RIS. Furthermore, the effect of the system parameters such as source power, eavesdropper distance and number of RIS cells on the system performance are investigated. Mathematical functions and notations are presented in Table I.

The paper is organized as follows. In Sections II and III, we describe the two system models under study and analyze the secrecy performance by deriving accurate analytical expressions for efficient computation of the secrecy capacity of the networks. Thereafter, in Sections IV and V, we present the results with discussions and outline the main conclusions, respectively.

Mathematical Functions and Notations

The following notations are used:

Notation	Definition
$\mathbb{E}[\cdot]$	Expectation operator
$G_{u,v}^{s,t}(x \dots)$	Meijer's G-function [42, Eq. (9.302)]
$\Gamma(z)$	$= \int_0^\infty t^{z-1} e^{-t} dt$, the gamma function [43, Eq. (8.310)]
$\text{erf}(x)$	$= \frac{2}{\sqrt{\pi}} \int_0^x e^{-t^2} dt$, the error function [43, Eq. (8.250.1)]
${}_2F_1(\alpha; \beta; \gamma; z)$	Gauss hypergeometric function [43, Eq. (9.111)]
$K_\nu(z)$	Modified Bessel function of the second kind and ν th order [43, Eq. (8.407)]
$\mathcal{M}_X(z)$	$= \mathbb{E}[e^{-zX}]$, the moment generating function of X .
$f(\gamma)$	Probability density function of γ .

¹This study will not go into detail on the process of mitigating doppler effects with RISs. The reader is however referred to [41] for a more detailed analysis.

II. V2V WITH RIS AS ACCESS POINT

In this section, we describe the V2V network with RIS as AP and derive expressions for the ASC and SOP of the system.

A. System Description

We consider a system of vehicles operating in a network as shown in Fig. 1. We assume a classic Wyner's wiretap model in our analysis [44], such that an information source vehicle (S), sends confidential information to a destination vehicle (D), while a passive eavesdropper vehicle (E) attempts to receive and decode the confidential information. The vehicles D and E are known to lie within a certain radius from S , the precise relative distances of the V2V links are unknown during transmission, which is a realistic assumption for a network of this nature [34], [45]. Moreover, S is assumed to employ a RIS-based scheme in the form of an AP to communicate over the network². As shown in the block diagram of Fig. 2, the RIS can be connected over a wired link or optical fiber for direct transmission from S , and can support transmission without RF processing. For the system considered, we assume an intelligent AP with the RIS having knowledge of channel phase terms, such that the RIS-induced phases can be adjusted to maximize the received SNR through appropriate phase cancellations and proper alignment of reflected signals from the intelligent surface.

The received signals at D and E are respectively represented as

$$y_D = \left[\sum_{n=1}^N h_{D,n} e^{-j\phi_n} \right] x + w_D, \quad (1)$$

$$y_E = \left[\sum_{n=1}^N h_{E,n} e^{-j\phi_n} \right] x + w_E, \quad (2)$$

where x represents the transmitted signal by S with power P_s , while the terms w_D and w_E are the respective additive white Gaussian noise (AWGN) at D and E , respectively. Without loss of generality, we denote the power spectral density of the AWGN as N_0 and equal at both links. The terms $h_{i,n} = \sqrt{g_{i,n} r_i^{-\beta}}$, $i \in \{D, E\}$, is the channel coefficient from S to the receiving vehicles D and E , where r_i is the V2V link distance, β is the path-loss exponent and $g_{i,n}$ is the channel gain from the RIS to the receiver, following independent double Rayleigh fading [34]. The term ϕ_n is the reconfigurable phase induced by the n th reflector of the RIS, which through phase matching, the SNR of the received signals can be maximized³. It is worth noting that the electromagnetic signal reconfiguration capability of the RIS is achieved by a joint phase control of individual RIS cells. It is possible to implement a type of software-defined control mechanism as proposed in [46], where tunable chips are integrated within the RIS cells, such that each chip communicates to a central controller [47], [48], or the RIS

²Initial proposal and results for such a configuration of intelligent surfaces employed as a transmitter or access point was reported in [7].

³For the sake of brevity, the reader is referred to [7], for details of phase cancellation mathematical techniques.

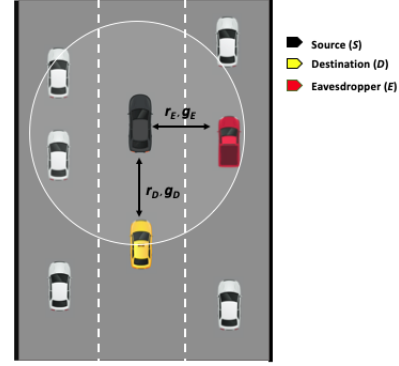


Figure 1: System model for V2V scenario with the source vehicle using RIS as AP.

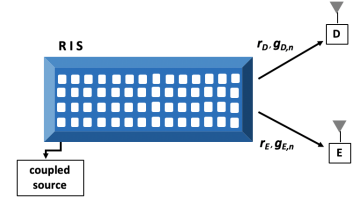


Figure 2: Vehicle RIS configuration as an AP.

could be fitted with sensors to receive for intelligent control, in-line with environmental factors [1].

Based on (1) and (2), the instantaneous SNRs at D and E are given by

$$\gamma_D = \frac{\sum_{n=1}^N P_s |h_{D,n}|^2}{N_0}, \quad (3)$$

and

$$\gamma_E = \frac{\sum_{n=1}^N P_s |h_{E,n}|^2}{N_0}. \quad (4)$$

B. Average Secrecy Capacity

In this section, we derive analytical expressions for the ASC of the system. The maximum achievable secrecy capacity is defined by [49]

$$C_s = \max \{C_D - C_E, 0\}, \quad (5)$$

where $C_D = \log_2(1 + \gamma_D)$ and $C_E = \log_2(1 + \gamma_E)$ are the instantaneous capacities of the main and eavesdropping links, respectively. The secrecy capacity in (5) can therefore be expressed as [49]

$$C_s = \begin{cases} \log_2(1 + \gamma_D) - \log_2(1 + \gamma_E), & \gamma_D > \gamma_E, \\ 0, & \gamma_D < \gamma_E. \end{cases} \quad (6)$$

The ASC $\overline{C_s}$ is given by [?]

$$\begin{aligned} \overline{C_s} &= \mathbb{E}[C_s(\gamma_D, \gamma_E)] \\ &= \int_0^\infty \int_0^\infty C_s(\gamma_D, \gamma_E) f(\gamma_D, \gamma_E) d\gamma_D d\gamma_E, \end{aligned} \quad (7)$$

where $\mathbb{E}[\cdot]$ is the expectation operator and $f(\gamma_D, \gamma_E)$ is the joint PDF of γ_D and γ_E . In order to simplify the analysis, we

express the logarithmic function in (5) in an alternate form. Recalling the identity [50, Eq. (6)]

$$\ln(1 + \zeta) = \int_0^{\infty} \frac{1}{s} (1 - e^{-\zeta s}) e^{-s} ds, \quad (8)$$

and by substituting $\zeta = \gamma_D$ in (8), we can express the instantaneous capacity of the main link as

$$\bar{C}_D = \frac{1}{\ln(2)} \int_0^{\infty} \frac{1}{z} (1 - \mathcal{M}_D(z)) e^{-z} dz, \quad (9)$$

where $\mathcal{M}_D(z) = \mathbb{E} \left[e^{-z \frac{P_s r_D^{-\beta}}{N_0} \sum_{n=1}^N g_{D,n}} \right]$ is the moment generating function (MGF) of the SNR at D .

Next, we compute the MGF $\mathcal{M}_D(z)$, defined by

$$\begin{aligned} \mathcal{M}_D(z) &= \mathbb{E} \left[e^{-z \frac{P_s r_D^{-\beta}}{N_0} \sum_{n=1}^N g_{D,n}} \right] \\ &= \prod_{n=1}^N \mathbb{E} \left[e^{-z \frac{P_s r_D^{-\beta}}{N_0} g_{D,n}} \right] \\ &= \prod_{n=1}^N \int_{g_D} e^{-z \xi_D g_{D,n}} f_{g_D}(g) dg_D, \end{aligned} \quad (10)$$

then from the generalized cascaded Rayleigh distribution, we can obtain the PDF of the double Rayleigh channel for $n = 2$ in [51, Eq. (8)] as $f(g) = G_{0,2}^{2,0} \left(\frac{1}{4} g^2 \middle| \frac{-}{\frac{1}{2}, \frac{1}{2}} \right)$. By invoking [43, Eq. (9.34.3)], we can express the PDF by re-writing the Meijer G-function in an alternate form. Thus, we get

$$f(g) = G_{0,2}^{2,0} \left(\frac{1}{4} g^2 \middle| \frac{-}{\frac{1}{2}, \frac{1}{2}} \right) = g K_0(g). \quad (11)$$

Using (11) and [43, Eq. (6.621.3)] along with some basic algebraic manipulations, we can obtain the desired result as

$$\mathcal{M}_D(z) = \prod_{n=1}^N \frac{4}{3(1 + z \frac{P_s r_D^{-\beta}}{N_0})^2} {}_2F_1 \left(2, \frac{1}{2}, \frac{5}{2}, \frac{z \frac{P_s r_D^{-\beta}}{N_0} - 1}{z \frac{P_s r_D^{-\beta}}{N_0} + 1} \right). \quad (12)$$

Using similar analysis, the average capacity of the eavesdropper link can be represented as

$$\bar{C}_E = \frac{1}{\ln(2)} \int_0^{\infty} \frac{1}{z} (1 - \mathcal{M}_E(z)) e^{-z} dz, \quad (13)$$

where the MGF $\mathcal{M}_E(z) = \mathbb{E} \left[e^{-z \frac{P_s r_E^{-\beta}}{N_0} \sum_{n=1}^N g_E} \right]$ and can be similarly evaluated as

$$\mathcal{M}_E(z) = \prod_{n=1}^N \frac{4}{3(1 + z \frac{P_s r_E^{-\beta}}{N_0})^2} {}_2F_1 \left(2, \frac{1}{2}, \frac{5}{2}, \frac{z \frac{P_s r_E^{-\beta}}{N_0} - 1}{z \frac{P_s r_E^{-\beta}}{N_0} + 1} \right). \quad (14)$$

From (6), (9), (12) - (14), the ASC can be represented as (15), shown at the top of the next page.

C. Approximate Secrecy Capacity

In this section, we present an approximate solution to the ASC computed in Sec. II-B, in order to provide a more direct solution. From (6), it can be seen that the secrecy capacity is defined as a logarithmic function. Thus, we can define an approximate bound to the solution in (15) by invoking Jensen's inequality⁴ [52, pp. 453] and applying to the expressions for the instantaneous capacities of the main and eavesdropping links. Therefore, the average capacity at D is

$$\begin{aligned} \mathbb{E}[\log_2(1 + \gamma_D)] &\leq \log_2(1 + \mathbb{E}[\gamma_D]) \\ &= \log_2 \left(1 + \mathbb{E} \left[\frac{P_s r_D^{-\beta}}{N_0} \sum_{n=1}^N g_{D,n} \right] \right) \\ &= \log_2 \left(1 + \frac{P_s r_D^{-\beta}}{N_0} \mathbb{E} \left[\sum_{n=1}^N g_{D,n} \right] \right), \end{aligned} \quad (16)$$

where γ_D is defined in (3). By using (11), the expectation in (16) can be obtained as

$$\begin{aligned} \mathbb{E} \left[\sum_{n=1}^N g_{D,n} \right] &= \int_0^{\infty} \sum_{n=1}^N g_{D,n} g_D K_0(g_D) dg_D \\ &\stackrel{(a)}{=} N \frac{\pi}{2}, \end{aligned} \quad (17)$$

where (a) in (17) was obtained with the aid of [43, Eq. (6.521.10)]. From (16) and (17), we obtain a bounded expression for the average capacity at D as

$$\bar{C}_D^{approx} = \log_2 \left(1 + \frac{N\pi P_s r_D^{-\beta}}{2N_0} \right). \quad (18)$$

Using similar analysis to the derivation of (18), we obtain a bounded expression for the average capacity at E as

$$\bar{C}_E^{approx} = \log_2 \left(1 + \frac{N\pi P_s r_E^{-\beta}}{2N_0} \right). \quad (19)$$

From (6), (18) and (19), we obtained the desired bounded expression as

$$\bar{C}_s^{approx} = \log_2 \left(\frac{2N_0 + N\pi P_s r_D^{-\beta}}{2N_0 + N\pi P_s r_E^{-\beta}} \right). \quad (20)$$

It is worth noting that, in addition to the fact that (20) lends itself much more easily to analysis as compared to (15), the expression (20) also produces highly accurate results for the parameters of interest, as will be demonstrated in the discussion in Sec. IV.

D. Secrecy Outage Probability

In this section, we derive an expression for the SOP of the V2V RIS AP model. The SOP is defined as the probability that the secrecy capacity falls below a target secrecy rate [35]. This can be represented as

$$P_o = \Pr[C_s < c_{th}] \quad (21)$$

⁴Jensen's inequality asserts that, if $f(x)$ is a convex function, then $\mathbb{E}[f(X)] \geq f(\mathbb{E}[X])$, provided that the expectations exist and are finite.

$$\bar{C}_s = \frac{1}{\ln(2)} \int_0^\infty \frac{1}{z} e^{-z} \left[\left(1 - \left\{ \frac{4}{3(N_0 + zP_s r_D^{-\beta})^2} {}_2F_1 \left(2, \frac{1}{2}, \frac{5}{2}, \frac{zP_s r_D^{-\beta} - N_0}{zP_s r_D^{-\beta} + N_0} \right) \right\} \right)^N - \left(1 - \left\{ \frac{4}{3(N_0 + zP_s r_E^{-\beta})^2} {}_2F_1 \left(2, \frac{1}{2}, \frac{5}{2}, \frac{zP_s r_E^{-\beta} - N_0}{zP_s r_E^{-\beta} + N_0} \right) \right\} \right)^N \right] dz. \quad (15)$$

where c_{th} is the pre-determined target secrecy rate. From (6) and (21) we obtain

$$\begin{aligned} P_o &= \Pr \left[\log_2 \left(\frac{1 + \gamma_D}{1 + \gamma_E} \right) < c_{\text{th}} \right] \\ &= \Pr \left[\frac{1 + \gamma_D}{1 + \gamma_E} < 2^{c_{\text{th}}} \right] \\ &\stackrel{(b)}{=} \Pr \left[P_s r_D^{-\beta} \sum_{n=1}^N g_{D,n} < \nu \left(N_0 + P_s r_E^{-\beta} \sum_{n=1}^N g_{E,n} \right) - N_0 \right] \\ &= \Pr \left[\sum_{n=1}^N g_{D,n} < \frac{\nu \left(N_0 + P_s r_E^{-\beta} \sum_{n=1}^N g_{E,n} \right) - N_0}{P_s r_D^{-\beta}} \right] \\ &\stackrel{(c)}{=} \Pr \left[\sum_{n=1}^N g_{D,n} < \underbrace{\frac{N_0(\nu - 1)}{P_s r_D^{-\beta}} + \frac{\nu r_E^{-\beta}}{r_D^{-\beta}} \sum_{n=1}^N g_{E,n}}_{\Theta} \right] \end{aligned} \quad (22)$$

where (b) follows from substituting (3) and (4) and $\nu = 2^{c_{\text{th}}}$. Given the difficulty in obtaining a tractable expression for the distribution of the sum $\sum_{n=1}^N g_{D,n}$ in (c) of (22), we employ an appropriate approximation using the central limit theorem (CLT) for reasonably large number of reflecting cells when $N \gg 1$. It therefore follows that $\sum_{n=1}^N g_{D,n}$ can be approximated by a Gaussian distribution with parameters; mean $\mu = N \frac{\pi}{2}$ (from (17)) and variance σ^2 given by

$$\begin{aligned} \text{Var} \left[\sum_{n=1}^N g_{D,n} \right] &= \mathbb{E} \left[\sum_{n=1}^N g_{D,n}^2 \right] - \mathbb{E} \left[\sum_{n=1}^N g_{D,n} \right]^2 \\ &= N \left(4 - \frac{\pi^2}{4} \right). \end{aligned} \quad (23)$$

Thus from (22), the SOP can be given by

$$P_o \approx \frac{1}{2} \left(1 + \text{erf} \left(\frac{\Theta - \mu}{\sqrt{2}\sigma} \right) \right), \quad (24)$$

where Θ is defined in (22) and $\mathbb{E}[\Theta]$ can be computed as

$$\begin{aligned} \mathbb{E}[\Theta] &= \mathbb{E} \left[\frac{N_0(\nu - 1)}{P_s r_D^{-\beta}} + \frac{\nu r_E^{-\beta}}{r_D^{-\beta}} \sum_{n=1}^N g_{E,n} \right] \\ &= \mathbb{E} \left[\frac{N_0(\nu - 1)}{P_s r_D^{-\beta}} + \frac{\nu r_E^{-\beta}}{r_D^{-\beta}} \sum_{n=1}^N g_{E,n} \right] \\ &\stackrel{(d)}{=} \frac{N_0(\nu - 1)}{P_s r_D^{-\beta}} + \frac{\nu N \pi r_E^{-\beta}}{2 r_D^{-\beta}}, \end{aligned} \quad (25)$$

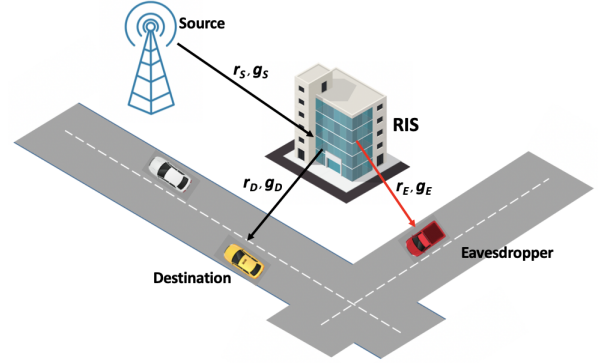


Figure 3: System model for a vehicular network scenario. Source station using building-mounted-RIS as relay for vehicular communication.

where (d) in (25) follows from (17) with $\mathbb{E} \left[\sum_{n=1}^N g_{E,n} \right] = N \frac{\pi}{2}$. The SOP for the V2V RIS access point is thus

$$P_o \approx \frac{1}{2} \left(1 + \text{erf} \left(\frac{\frac{N_0(\nu-1)}{P_s r_D^{-\beta}} + N \frac{\pi}{2} \left(\frac{\nu r_E^{-\beta}}{r_D^{-\beta}} - 1 \right)}{\sqrt{2N \left(4 - \frac{\pi^2}{4} \right)}} \right) \right). \quad (26)$$

III. VANET TRANSMISSION THROUGH RIS RELAY

In this section, we describe the VANET system transmitting through a RIS relay and derive expressions for the ASC and SOP of the system.

A. System Description

In this section, we consider an RIS-based scheme with the RIS employed as a relay or reflector for vehicular nodes in the network. Fig. 3 illustrates the RIS-based system under consideration. The RIS is deployed on a building and used as a relay for the signal from stationary source S , while D and E are assumed to be highly mobile vehicular nodes. Under this assumption, the source-to-RIS channel g_s is assumed to be Rayleigh faded, while the RIS-to-destination and RIS-to-eavesdropper fading channels, g_D and g_E are assumed to be double-Rayleigh distributed. The RIS is in the form of a reflect-array comprising N reconfigurable reflector elements, capable of being controlled by a communication oriented software for intelligent transmission. With this in mind, the received signals at D and E are

$$y_i = \left[\sum_{n=1}^N h_s h_{i,n} e^{-j\phi_n} \right] x + w_i, i \in \{D, E\}, \quad (27)$$

where $h_{s,n} = \sqrt{g_{s,n} r_s^{-\beta}} e^{-j\theta_n}$ is the source-to-RIS channel with distance r_s , phase component θ_n and g_s following a Rayleigh fading distribution. The term $h_{i,n} = \sqrt{g_{i,n} r_i^{-\beta}} e^{-j\psi_n}$, $i \in \{D, E\}$, is the channel coefficient from RIS-to-vehicle node, with distance r_i , path-loss exponent β , phase component ψ_n and $g_{i,n}$ following a double-Rayleigh distribution to model the mobility of the nodes [34]. The instantaneous SNRs at D and E are given respectively by

$$\gamma_D^r = \frac{\sum_{n=1}^N P_s |h_{s,n}|^2 |h_{D,n}|^2}{N_0} \quad (28)$$

and

$$\gamma_E^r = \frac{\sum_{n=1}^N P_s |h_{s,n}|^2 |h_{E,n}|^2}{N_0} \quad (29)$$

B. Average Secrecy Capacity Analysis

From (9), we obtain the average capacity for the destination V2V link as

$$\bar{C}_{D,r} = \frac{1}{\ln(2)} \int_0^\infty \frac{1}{z} (1 - \mathcal{M}_{D,r}(z)) e^{-z} dz, \quad (30)$$

where $\mathcal{M}_{D,r}(z) = \mathbb{E} \left[e^{-z \frac{P_s r_s^{-\beta} r_D^{-\beta}}{N_0} \sum_{n=1}^N g_{s,n} g_{D,n}} \right]$ is the MGF of the SNR at D . As for the joint distribution of g_s and g_D , given that g_s is a Rayleigh RV and g_D is a double-Rayleigh RV, we can define the RV $g = g_s g_D$, which follows the cascaded Rayleigh distribution with $n = 3$. From the generalized cascaded Rayleigh distribution [51], we can evaluate the PDF of g as

$$f(g) = \frac{1}{\sqrt{2}} G_{0,3}^{3,0} \left(\frac{1}{8} g^2 \middle| \begin{matrix} - \\ \frac{1}{2}, \frac{1}{2}, \frac{1}{2} \end{matrix} \right). \quad (31)$$

Thus, the $\mathcal{M}_{D,r}(z)$ is given by

$$\begin{aligned} \mathcal{M}_{D,r}(z) &= \mathbb{E} \left[e^{-z \frac{P_s r_s^{-\beta} r_D^{-\beta}}{N_0} \sum_{n=1}^N g_{s,n} g_{D,n}} \right] \\ &= \prod_{n=1}^N \int_0^\infty e^{-z g \frac{P_s r_s^{-\beta} r_D^{-\beta}}{N_0}} f_g(g) dg \\ &= \prod_{n=1}^N \int_0^\infty \frac{1}{\sqrt{2}} e^{-z g \frac{P_s r_s^{-\beta} r_D^{-\beta}}{N_0}} G_{0,3}^{3,0} \left(\frac{1}{8} g^2 \middle| \begin{matrix} - \\ \frac{1}{2}, \frac{1}{2}, \frac{1}{2} \end{matrix} \right) dg. \end{aligned} \quad (32)$$

Using (31) and [43, Eq. (7.813.2)] along with some basic algebraic manipulations, we can obtain the MGF as

$$\mathcal{M}_{D,r}(z) = \prod_{n=1}^N \frac{1}{z \mu_d \sqrt{2\pi}} G_{2,3}^{3,2} \left(\frac{1}{2(z\mu_d)^2} \middle| \begin{matrix} 0, \frac{1}{2} \\ \frac{1}{2}, \frac{1}{2}, \frac{1}{2} \end{matrix} \right), \quad (33)$$

where $\mu_d = \frac{P_s r_s^{-\beta} r_D^{-\beta}}{N_0}$. Using similar analysis, the average capacity of the eavesdropper link can be represented as

$$\bar{C}_{E,r} = \frac{1}{\ln(2)} \int_0^\infty \frac{1}{z} (1 - \mathcal{M}_{E,r}(z)) e^{-z} dz, \quad (34)$$

where the MGF $\mathcal{M}_{E,r}(z) = \mathbb{E} \left[e^{-z \frac{P_s r_s^{-\beta} r_E^{-\beta}}{N_0} \sum_{n=1}^N g_{s,n} g_{E,n}} \right]$ and can be similarly evaluated as

$$\mathcal{M}_{E,r}(z) = \prod_{n=1}^N \frac{1}{z \mu_e \sqrt{2\pi}} G_{2,3}^{3,2} \left(\frac{1}{2(z\mu_e)^2} \middle| \begin{matrix} 0, \frac{1}{2} \\ \frac{1}{2}, \frac{1}{2}, \frac{1}{2} \end{matrix} \right), \quad (35)$$

where $\mu_e = \frac{P_s r_s^{-\beta} r_E^{-\beta}}{N_0}$.

From (6), (30), (33) - (35), the ASC can be represented as (36), shown at the top of the next page.

C. Approximate Secrecy Capacity

In this section, we present an approximate expression to the ASC for the VANET transmission through RIS relay, as computed in Sec. III-B. Following similar analysis to the derivation of an approximate expression in Sec. II-C, we invoke Jensen's inequality to obtain a bound for the expression in (36). We commence with the average capacity at D , which can be approximated as

$$\begin{aligned} \mathbb{E} [\log_2(1 + \gamma_D^r)] &\leq \log_2(1 + \mathbb{E}[\gamma_D^r]) \\ &= \log_2 \left(1 + \mathbb{E} \left[\frac{P_s r_s^{-\beta} r_D^{-\beta}}{N_0} \sum_{n=1}^N g_{s,n} g_{D,n} \right] \right) \\ &= \log_2 \left(1 + \frac{P_s r_s^{-\beta} r_D^{-\beta}}{N_0} \mathbb{E} \left[\sum_{n=1}^N g_{s,n} g_{D,n} \right] \right), \end{aligned} \quad (37)$$

where γ_D^r is defined in (28), as the instantaneous SNR at D for the VANET RIS relay network. Given that the channels g_s and g_D are independent, then the expectation in (37) can be obtained as

$$\begin{aligned} \mathbb{E} \left[\sum_{n=1}^N g_{s,n} g_{D,n} \right] &= \sum_{n=1}^N \mathbb{E}[g_{s,n}] \mathbb{E}[g_{D,n}] \\ &\stackrel{(d)}{=} \int_0^\infty \int_0^\infty \sum_{n=1}^N g_s^2 g_D^2 K_0(g_D) e^{-\frac{g_s^2}{2}} dg_D dg_s \\ &\stackrel{(e)}{=} N \left(\frac{\pi}{2} \right)^{\frac{3}{2}}, \end{aligned} \quad (38)$$

where (d) in (38) was obtained using (11) and the fact that g_s is Rayleigh distributed with PDF $f(g_s) = g_s \exp(-\frac{1}{2}g_s^2)$, while (e) was obtained with the aid of [43, Eqs. (6.521.10) and (3.326.2)]. From (37) and (38), we obtain a bounded expression for the average capacity at D for the VANET RIS relay as

$$\bar{C}_{D,r}^{appr} = \log_2 \left(1 + \frac{NP_s (\pi)^{\frac{3}{2}} r_s^{-\beta} r_D^{-\beta}}{2\sqrt{2}N_0} \right). \quad (39)$$

Using similar analysis to the derivation of (39), we obtain a bounded expression for the average capacity at E for the VANET RIS relay as

$$\bar{C}_{E,r}^{appr} = \log_2 \left(1 + \frac{NP_s (\pi)^{\frac{3}{2}} r_s^{-\beta} r_E^{-\beta}}{2\sqrt{2}N_0} \right). \quad (40)$$

$$\bar{C}_{s,r} = \frac{1}{\ln(2)} \int_0^\infty \frac{1}{z} e^{-z} \left[\left(1 - \left\{ \frac{N_0}{\sqrt{2\pi} z P_s r_s^{-\beta} r_D^{-\beta}} \mathbf{G}_{2,3}^{3,2} \left(\frac{1}{2} \left(\frac{N_0}{z P_s r_s^{-\beta} r_D^{-\beta}} \right)^2 \middle| \begin{matrix} 0, \frac{1}{2} \\ \frac{1}{2}, \frac{1}{2}, \frac{1}{2} \end{matrix} \right) \right\} \right)^N - \left(1 - \left\{ \frac{N_0}{z P_s r_s^{-\beta} r_E^{-\beta} \sqrt{2\pi}} \mathbf{G}_{2,3}^{3,2} \left(\frac{1}{2} \left(\frac{N_0}{z P_s r_s^{-\beta} r_E^{-\beta}} \right)^2 \middle| \begin{matrix} 0, \frac{1}{2} \\ \frac{1}{2}, \frac{1}{2}, \frac{1}{2} \end{matrix} \right) \right\} \right)^N \right] dz. \quad (36)$$

From (6), (39) and (40), we obtained the desired bounded expression for the VANET RIS relay as

$$\bar{C}_{s,r}^{apprx} = \log_2 \left(\frac{2\sqrt{2}N_0 + NP_s (\pi)^{\frac{3}{2}} r_s^{-\beta} r_D^{-\beta}}{2\sqrt{2}N_0 + NP_s (\pi)^{\frac{3}{2}} r_s^{-\beta} r_E^{-\beta}} \right). \quad (41)$$

The accuracy of (41) as compared to the exact analytical solution in (36) will be demonstrated in the discussion in Sec. IV.

D. Secrecy Outage Probability

In this section, we derive an expression for the SOP of the VANET RIS relay system. Similar to the derivation in Sec. II-D, from (6) and (21) we obtain

$$\begin{aligned} P_o^r &= \Pr \left[\log_2 \left(\frac{1 + \gamma_D}{1 + \gamma_E} \right) < c_{th} \right] \\ &= \Pr \left[\frac{1 + \gamma_D}{1 + \gamma_E} < 2^{c_{th}} \right] \\ &\stackrel{(f)}{=} \Pr \left[P_s r_s^{-\beta} r_D^{-\beta} \sum_{n=1}^N g_{s,n} g_{D,n} < \right. \\ &\quad \left. \nu \left(N_0 + P_s r_s^{-\beta} r_E^{-\beta} \sum_{n=1}^N g_{s,n} g_{E,n} \right) - N_0 \right] \\ &\stackrel{(g)}{=} \Pr \left[\sum_{n=1}^N g_{s,n} g_{D,n} < \underbrace{\frac{N_0 (\nu - 1)}{P_s r_s^{-\beta} r_D^{-\beta}} + \frac{\nu r_E^{-\beta}}{r_D^{-\beta}} \sum_{n=1}^N g_{s,n} g_{E,n}}_{\Theta_r} \right] \end{aligned} \quad (42)$$

where $\nu = 2^{c_{th}}$ and (f) follows from (28) and (29). Owing to the difficulty in obtaining a direct expression for the distribution of the sum $\sum_{n=1}^N g_{s,n} g_{D,n}$ in (g) of (42), we employ the CLT to approximate with a Gaussian distribution with parameters; mean $\mu_r = N \left(\frac{\pi}{2} \right)^{\frac{3}{2}}$ (from (38)) and variance σ_r^2 given by

$$\begin{aligned} \text{Var} \left[\sum_{n=1}^N g_{s,n} g_{D,n} \right] &= \mathbb{E} \left[\sum_{n=1}^N g_{s,n}^2 g_{D,n}^2 \right] - \mathbb{E} \left[\sum_{n=1}^N g_{s,n} g_{D,n} \right]^2 \\ &= N \left(8 - \left(\frac{\pi}{2} \right)^{\frac{3}{2}} \right). \end{aligned} \quad (43)$$

Thus from (42), the SOP can be given by

$$P_o \approx \frac{1}{2} \left(1 + \text{erf} \left(\frac{\Theta_r - \mu_r}{\sqrt{2}\sigma_r} \right) \right), \quad (44)$$

where Θ_r is defined in (42) and $\mathbb{E}[\Theta_r]$ can be computed as

$$\begin{aligned} \mathbb{E}[\Theta_r] &= \mathbb{E} \left[\frac{N_0 (\nu - 1)}{P_s r_s^{-\beta} r_D^{-\beta}} + \frac{\nu r_E^{-\beta}}{r_D^{-\beta}} \sum_{n=1}^N g_{s,n} g_{E,n} \right] \\ &= \mathbb{E} \left[\frac{N_0 (\nu - 1)}{P_s r_s^{-\beta} r_D^{-\beta}} + \frac{\nu r_E^{-\beta}}{r_D^{-\beta}} \sum_{n=1}^N g_{s,n} g_{E,n} \right] \\ &\stackrel{(h)}{=} \frac{N_0 (\nu - 1)}{P_s r_s^{-\beta} r_D^{-\beta}} + \frac{\nu N \pi^3 r_E^{-\beta}}{2\sqrt{2} r_D^{-\beta}}, \end{aligned} \quad (45)$$

where (h) in (45) follows from (38) with $\mathbb{E} \left[\sum_{n=1}^N g_{s,n} g_{E,n} \right] = \frac{N \pi^3}{2\sqrt{2}}$. The SOP for the VANET RIS relay system is therefore

$$P_o^r \approx \frac{1}{2} \left(1 + \text{erf} \left(\frac{\frac{N_0 (\nu - 1)}{P_s r_s^{-\beta} r_D^{-\beta}} + \frac{N \pi^3}{2\sqrt{2}} \left(\frac{\nu r_E^{-\beta}}{r_D^{-\beta}} - 1 \right)}{\sqrt{2N \left(8 - \left(\frac{\pi}{2} \right)^{\frac{3}{2}} \right)}} \right) \right). \quad (46)$$

IV. NUMERICAL RESULTS AND DISCUSSIONS

In this section, we present and discuss some results from the mathematical expressions derived in the paper. We then investigate the effects of key parameters on the secrecy capacity of the system. The results are then verified using Monte Carlo simulations with at least 10^4 iterations. Unless otherwise stated, we have assumed source power $P_s = 10\text{W}$, RIS-to- D distance $r_D = 4\text{m}$, RIS-to- E distance $r_E = 8\text{m}$, source-to-RIS distance $r_s = 10\text{m}$, secrecy outage threshold $c_{th} = 1$ bit/Hz and path loss exponent $\beta = 2.7$.

A. Average Secrecy Capacity

In this subsection, we examine the ASC of both system models considered. In Fig. 4, we commence analysis for the V2V network model, with the ASC against source power for different numbers of RIS cells and eavesdropper distances. It can be observed that the secrecy capacity increases with an increase in P_s , r_E or N . It can be further noted that within the region considered, the eavesdropper distance has a greater effect on the secrecy capacity than doubling the number of RIS cells. Also, the effect of increased RIS cells, is more pronounced when the eavesdropper is further away. A similar analysis can be made for the ASC of the VANET RIS-relay model considered, as observed in Fig. 5. However, the effect of increased source power produces an almost linear response for the secrecy capacity, while the effective value of the secrecy capacity is much lower than the V2V RIS model for similar

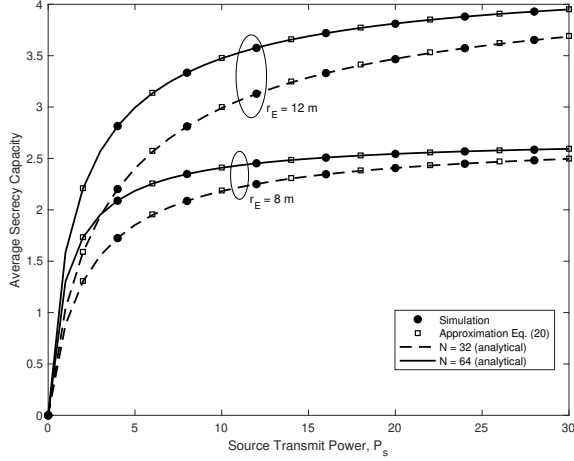


Figure 4: Average secrecy capacity versus source transmit power P_s for the V2V network with RIS as AP. Parameters considered with varying eavesdropper distance r_E and number of RIS cells N .

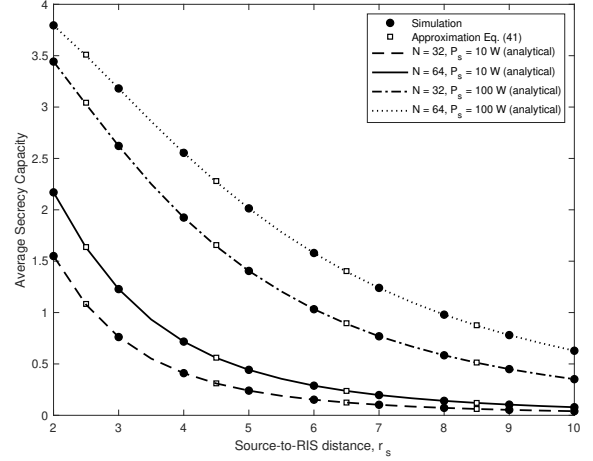


Figure 6: Average secrecy capacity versus source-to-RIS distance for the VANET with RIS as relay. Parameters considered with varying source transmit power P_s and number of RIS cells N .

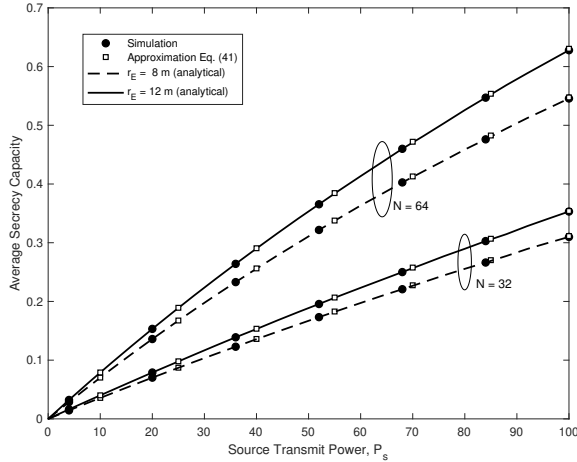


Figure 5: Average secrecy capacity versus source transmit power P_s for the VANET with RIS as relay. Parameters considered with varying eavesdropper distance r_E and number of RIS cells N .

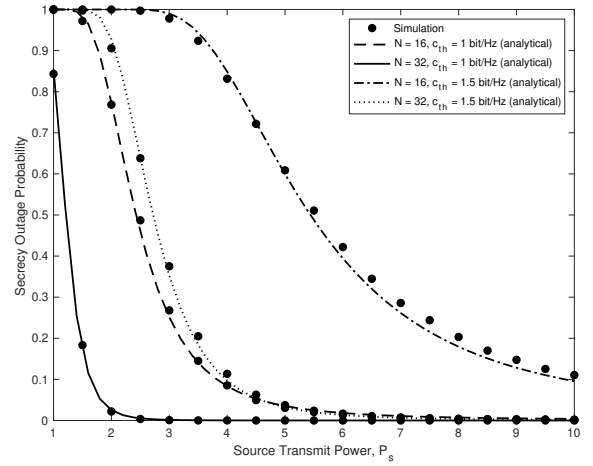


Figure 7: Secrecy outage probability versus source transmit power P_s for the V2V network with RIS as AP. Parameters considered with varying secrecy capacity threshold c_{th} and number of RIS cells N .

P_s . In both Figs. 4 and 5, it can also be observed that the analytical results in (20) and (41) provide highly accurate approximations for the secrecy capacity of the V2V RIS model and VANET RIS-relay model respectively.

Fig. 6, shows a plot of the ASC against r_s with different values of P_s and N , for the VANET RIS-relay system. We assume the RIS-to-eavesdropper distance to be $r_E = 12$ m. First, we observe that the ASC decreases as the source distance increases, demonstrating the effect of fading and path loss on the link, before the RIS relay.

The result also demonstrates that doubling the number of RIS cells has less influence on the ASC, as compared to the impact of the source power, within the observed region. Furthermore, we again observe the high accuracy of the approximate expressions in (41), within the regions of interest studied in these results.

B. Average Secrecy Outage Probability

In this subsection, we present results for the average SOP of both systems considered from the expressions derived. In Fig. 7, the SOP of the V2V RIS access point is plotted against the source transmit power for different threshold values and numbers of RIS cells. From the plot, we observe that the SOP decreases with increased transmit power or increase number of RIS cells, resulting from stronger SNR conditions. On the other hand, the SOP is proportional to the threshold within the region investigated, as expected. We can particularly observe that the SOP performance is affected more significantly when the threshold is at 1.5 bit/Hz compared to 1 bit/Hz, such that over half an order of magnitude gain in performance is possible, when the RIS cells are doubled from $N = 16$ to 32, in some regions of operation for this system model.

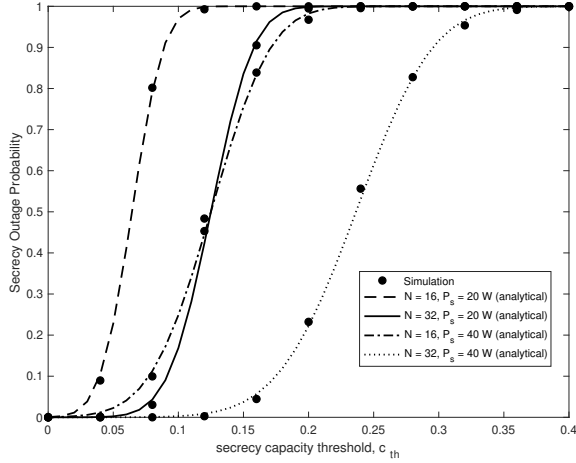


Figure 8: Secrecy outage probability versus secrecy capacity threshold c_{th} for the VANET with RIS as relay. Parameters considered with varying source transmit power P_s and number of RIS cells N .

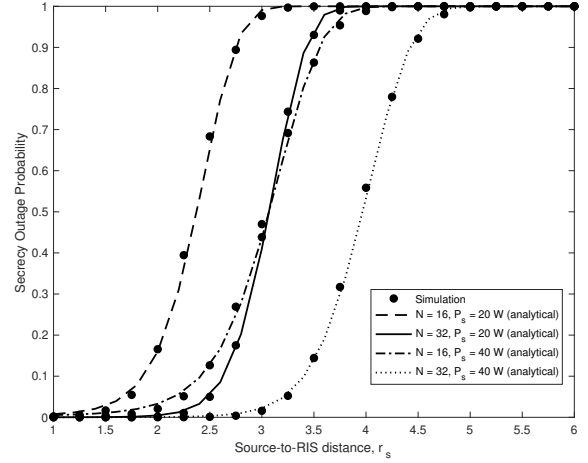


Figure 9: Secrecy outage probability versus source-to-RIS distance for the VANET with RIS as relay. Parameters considered with varying source transmit power P_s and number of RIS cells N .

The effect of the system parameters on the SOP for the VANET with RIS relay system is illustrated in Figs. 8 and 9. In Fig. 8, the SOP for the VANET with RIS is plotted against the expected secrecy threshold, for different values of source transmit power and number of RIS cells. It can be observed that for this model, the system performance is degraded (increased SOP) when we adopt higher threshold values for all corresponding values of N and P_s . It is interesting to see that, the effect of doubling the number of cells from $N = 16$ to 32 at a fixed transmit power is more pronounced than doubling the power from $P_s = 20$ to 40 W, with respect to the SOP. In Fig. 9, the SOP for the VANET with RIS is plotted against the source-to-RIS distance, where the SOP curves show decreased performance when r_s increases and that the SOP rapidly degrades within a short distance. For example, it can be shown that within the regions observed, the SOP falls by about an order of magnitude (from SOP = 1 to 0.1) for a change of less than 2 m. Moreover, we observe in this case, the effect of changing $N = 16$ to 32 at a fixed transmit power is similar to increasing the power from $P_s = 20$ to 40 W, with respect to the SOP.

Therefore, from a practical perspective, the results in Figs. 8 and 9 indicate that there is a design decision to consider the cost versus benefit of extra hardware required to double the RIS cells or the source transmit power, while noting that for some applications the number of RIS cells could be much larger than 100. (i.e. $N \gg 100$).

V. CONCLUSIONS

In this paper, we examined the effects of key parameters on the PLS of a wireless vehicular communication network. As a novel study on the subject, two scenarios of a RIS-based vehicular network were considered. The results demonstrate how the secrecy capacity and SOP of a vehicular network can be improved with respect to the source power, eavesdropper

distance, the number of RIS cells, the source-to-relay distance and the secrecy threshold. The results further showed how the location and size of RIS (in terms of number of RIS cells) can be employed to improve a RIS relay-based VANET, while clearly indicating the benefits of employing the RIS in all cases.

REFERENCES

- [1] M. D. Renzo, M. Debbah, D.-T. Phan-Huy, A. Zappone, M.-S. Alouini, C. Yuen, V. Sciancalepore, G. C. Alexandropoulos, J. Hoydis, H. Gacanin, J. d. Rosny, A. Bounceur, G. Lerosey, and M. Fink, "Smart radio environments empowered by reconfigurable AI meta-surfaces: An idea whose time has come," *EURASIP J. Wireless Commun. Netw.*, vol. 2019, no. 1, p. 129, May 2019. [Online]. Available: <https://doi.org/10.1186/s13638-019-1438-9>
- [2] C. Liaskos, S. Nie, A. Tsioliariidou, A. Pitsillides, S. Ioannidis, and I. Akyildiz, "A new wireless communication paradigm through software-controlled metasurfaces," *IEEE Commun. Mag.*, vol. 56, no. 9, pp. 162–169, Sep. 2018.
- [3] E. Basar, M. D. Renzo, J. D. Rosny, M. Debbah, M.-S. Alouini, and R. Zhang, "Wireless communications through reconfigurable intelligent surfaces," *IEEE Access*, vol. 7, pp. 116 753–116 773, 2019.
- [4] S. Gong, X. Lu, D. T. Hoang, D. Niyato, L. Shu, D. I. Kim, and Y.-C. Liang, "Towards smart radio environment for wireless communications via intelligent reflecting surfaces: A comprehensive survey," arXiv:1912.07794, Dec. 2019. [online]. Available: <https://arxiv.org/abs/1912.07794>.
- [5] C. Huang, S. Hu, G. C. Alexandropoulos, A. Zappone, C. Yuen, R. Zhang, M. D. Renzo, and M. Debbah, "Holographic mimo surfaces for 6g wireless networks: Opportunities, challenges, and trends," arXiv:1911.12296, Dec. 2019. [online]. Available: <https://arxiv.org/abs/1911.12296>.
- [6] Y.-C. Liang, R. Long, Q. Zhang, J. Chen, H. V. Cheng, and H. Guo, "Large Intelligent Surface/Antennas (LISA): Making Reflective Radios Smart," arXiv:1906.06578, Dec. 2019. [online]. Available: <https://arxiv.org/abs/1906.06578>.
- [7] E. Basar, "Transmission Through Large Intelligent Surfaces: A New Frontier in Wireless Communications," in *2019 European Conf. Netw. Commun. (EuCNC)*, Jun. 2019, pp. 112–117.
- [8] A. U. Makarfi, K. M. Rabie, O. Kaiwartya, O. S. Badarneh, X. Li, and R. Kharel, "Reconfigurable intelligent surface enabled IoT networks in generalized fading channels," arXiv:1912.06250, Dec. 2019. [online]. Available: <https://arxiv.org/abs/1912.06250>.
- [9] O. Ozdogan, E. Bjornson, and E. G. Larsson, "Intelligent reflecting surfaces: Physics, propagation, and pathloss modeling," *IEEE Wireless Commun. Lett.*, pp. 1–1, 2019, Early Access.

- [10] M. Najafi and R. Schober, "Intelligent reflecting surfaces for free space optical communications," in *IEEE Global Commun. Conf. (GLOBECOM)*, Dec 2019, pp. 1–6.
- [11] C. Huang, G. C. Alexandropoulos, A. Zappone, M. Debbah, and C. Yuen, "Energy efficient multi-user MISO communication using low resolution large intelligent surfaces," in *IEEE Global Commun. Conf. Workshops (GC Wkshps)*, Dec. 2018, pp. 1–6.
- [12] C. Huang, A. Zappone, G. C. Alexandropoulos, M. Debbah, and C. Yuen, "Reconfigurable intelligent surfaces for energy efficiency in wireless communication," *IEEE Trans. Wireless Commun.*, vol. 18, pp. 4157–4170, 2018.
- [13] L. Subrt and P. Pechac, "Controlling propagation environments using intelligent walls," in *6th European Conf. Antennas Propag. (EUCAP)*, Mar. 2012, pp. 1–5.
- [14] S. Hu, F. Rusek, and O. Edfors, "Beyond Massive MIMO: The Potential of Data Transmission With Large Intelligent Surfaces," *IEEE Trans. Sig. Process.*, vol. 66, no. 10, pp. 2746–2758, May 2018.
- [15] —, "Beyond massive MIMO: The potential of positioning with large intelligent surfaces," *IEEE Trans. Sig. Process.*, vol. 66, no. 7, pp. 1761–1774, Apr. 2018.
- [16] A. Taha, M. Alrabeiah, and A. Alkhateeb, "Deep learning for large intelligent surfaces in millimeter wave and massive MIMO systems," in *IEEE Global Commun. Conf. (GLOBECOM)*, Dec 2019, pp. 1–6.
- [17] H.-T. Chen, A. J. Taylor, and N. Yu, "A review of metasurfaces: physics and applications," *Reports on Progress in Physics*, vol. 79, p. 076401, Jun 2016. [Online]. Available: <http://dx.doi.org/10.1088/0034-4885/79/7/076401>
- [18] C. L. Holloway, E. F. Kuester, J. A. Gordon, J. O'Hara, J. Booth, and D. R. Smith, "An overview of the theory and applications of metasurfaces: The two-dimensional equivalents of metamaterials," *IEEE Ant. Propag. Mag.*, vol. 54, no. 2, pp. 10–35, Apr. 2012.
- [19] Q. Wu and R. Zhang, "Beamforming optimization for intelligent reflecting surface with discrete phase shifts," in *IEEE Int. Conf. Acoust., Speech and Sig. Process. (ICASSP)*, May 2019, pp. 7830–7833.
- [20] —, "Intelligent reflecting surface enhanced wireless network: Joint active and passive beamforming design," in *IEEE Global Commun. Conf. (GLOBECOM)*, Dec. 2018, pp. 1–6.
- [21] X. Tan, Z. Sun, J. M. Jornet, and D. Pados, "Increasing indoor spectrum sharing capacity using smart reflect-array," in *IEEE Int. Conf. Commun. (ICC)*, May 2016, pp. 1–6.
- [22] Q. Wu and R. Zhang, "Intelligent reflecting surface enhanced wireless network via joint active and passive beamforming," *IEEE Trans. Wireless Commun.*, vol. 18, no. 11, pp. 5394–5409, Nov. 2019.
- [23] Y. Liu, L. Zhang, B. Yang, W. Guo, and M. A. Imran, "Programmable wireless channel for multi-user MIMO transmission using meta-surface," in *IEEE Global Commun. Conf. (GLOBECOM)*, Dec 2019, pp. 1–6.
- [24] C. Huang, A. Zappone, M. Debbah, and C. Yuen, "Achievable Rate Maximization by Passive Intelligent Mirrors," in *IEEE Int. Conf. Acoust. Speech Sig. Process. (ICASSP)*, Apr. 2018, pp. 3714–3718.
- [25] M. Cui, G. Zhang, and R. Zhang, "Secure wireless communication via intelligent reflecting surface," *IEEE Wireless Commun. Lett.*, pp. 1–1, 2019.
- [26] J. Chen, Y.-C. Liang, Y. Pei, and H. Guo, "Intelligent Reflecting Surface: A Programmable Wireless Environment for Physical Layer Security," *IEEE Access*, vol. 7, pp. 82 599–82 612, 2019.
- [27] X. Yu, D. Xu, and R. Schober, "Enabling secure wireless communications via intelligent reflecting surfaces," in *IEEE Global Commun. Conf. (GLOBECOM)*, Dec 2019, pp. 1–6.
- [28] Z. Chu, W. Hao, P. Xiao, and J. Shi, "Intelligent reflecting surface aided multi-antenna secure transmission," *IEEE Wireless Commun. Lett.*, pp. 1–1, 2019, Early Access.
- [29] H. Shen, W. Xu, S. Gong, Z. He, and C. Zhao, "Secrecy rate maximization for intelligent reflecting surface assisted multi-antenna communications," *IEEE Commun. Lett.*, vol. 23, no. 9, pp. 1488–1492, Sep. 2019.
- [30] I. Dey, R. Nagraj, G. G. Messier, and S. Magierowski, "Performance analysis of relay-assisted mobile-to-mobile communication in double or cascaded Rayleigh fading," in *IEEE Pacific Rim Conf. Commun. Comput. Sign. Process.*, Aug. 2011, pp. 631–636.
- [31] R. Kasana, S. Kumar, O. Kaiwartya, R. Kharel, J. Lloret, N. Aslam, and T. Wang, "Fuzzy-based channel selection for location oriented services in multichannel VCPS environments," *IEEE Internet Things J.*, vol. 5, no. 6, pp. 4642–4651, Dec 2018.
- [32] O. Kaiwartya, Y. Cao, J. Lloret, S. Kumar, N. Aslam, R. Kharel, A. H. Abdullah, and R. R. Shah, "Geometry-Based Localization for GPS Outage in Vehicular Cyber Physical Systems," *IEEE Trans. Veh. Tech.*, vol. 67, no. 5, pp. 3800–3812, May 2018.
- [33] S. Kumar, U. Dohare, K. Kumar, D. Prasad, K. N. Qureshi, and R. Kharel, "Cybersecurity measures for geocasting in vehicular cyber physical system environments," *IEEE Internet Things J.*, pp. 1–1, 2019.
- [34] Y. Ai, M. Cheffena, A. Mathur, and H. Lei, "On Physical Layer Security of Double Rayleigh Fading Channels for Vehicular Communications," *IEEE Wireless Commun. Lett.*, vol. 7, no. 6, pp. 1038–1041, Dec. 2018.
- [35] A. U. Makarfi, R. Kharel, K. M. Rabie, O. Kaiwartya, and G. Naurzybayev, "Physical Layer Security in Vehicular Communication Networks in the Presence of Interference," in *IEEE Global Commun. Conf. (GLOBECOM)*, Dec. 2019, pp. 1–6.
- [36] A. Pandey and S. Yadav, "Physical layer security in cooperative af relaying networks with direct links over mixed rayleigh and double-rayleigh fading channels," *IEEE Trans. Veh. Tech.*, vol. 67, no. 11, pp. 10 615–10 630, Nov. 2018.
- [37] L. Xu, X. Yu, H. Wang, X. Dong, Y. Liu, W. Lin, X. Wang, and J. Wang, "Physical layer security performance of mobile vehicular networks," *Mobile Neww. Appl.*, pp. 1–7, Apr. 2019.
- [38] A. Pandey and S. Yadav, "Performance evaluation of amplify and forward relaying cooperative vehicular networks under physical layer security," *Trans. Emerging Telecommun. Technol.*, vol. 29, no. 12, p. e3534, Oct. 2018.
- [39] M. Jung, W. Saad, Y. R. Jang, G. Kong, and S. Choi, "Performance Analysis of Large Intelligence Surfaces (LISs): Asymptotic Data Rate and Channel Hardening Effects," *ArXiv*, vol. abs/1810.05667, 2018.
- [40] Y. M. Khattabi and M. M. Matalgah, "Performance Analysis of Multiple-Relay AF Cooperative Systems Over Rayleigh Time-Selective Fading Channels With Imperfect Channel Estimation," *IEEE Trans. Veh. Technol.*, vol. 65, no. 1, pp. 427–434, Jan. 2016.
- [41] E. Basar and I. F. Akyildiz, "Reconfigurable Intelligent Surfaces for Doppler Effect and Multipath Fading Mitigation," arXiv:1912.04080v1, Dec. 2019. [online]. Available: <https://arxiv.org/abs/1912.04080v1>.
- [42] A. P. Prudnikov, Y. A. Brychkov, and O. I. Marichev, *Integrals, and Series: More Special Functions*, Gordon and Breach Sci. Publ., New York, 1990, vol. 3.
- [43] I. S. Gradshteyn and I. M. Ryzhik, *Table of Integrals, Series, and Products*. California: Academic Press, 7th ed., 2007.
- [44] H. Lei, I. S. Ansari, G. Pan, B. Alomair, and M. Alouini, "Secrecy Capacity Analysis Over α - μ Fading Channels," *IEEE Commun. Lett.*, vol. 21, no. 6, pp. 1445–1448, Jun. 2017.
- [45] D. S. Karas, A. A. Boulogeorgos, and G. K. Karagiannidis, "Physical layer security with uncertainty on the location of the eavesdropper," *IEEE Wireless Commun. Lett.*, vol. 5, no. 5, pp. 540–543, Oct. 2016.
- [46] C. Liaskos, A. Tsiolaridou, A. Pitsillides, I. F. Akyildiz, N. V. Kantartzis, A. X. Lalas, X. Dimitropoulos, S. Ioannidis, M. Kafesaki, and C. M. Soukoulis, "Design and development of software defined metamaterials for nanonetworks," *IEEE Circuits Syst. Mag.*, vol. 15, no. 4, pp. 12–25, Fourthquarter 2015.
- [47] F. Liu, A. Ptilakis, M. S. Mirmoosa, O. Tsilipakos, X. Wang, A. C. Tasolamprou, S. Abadal, A. Cabellos-Aparicio, E. Alarcon, C. Liaskos, N. V. Kantartzis, M. Kafesaki, E. N. Economou, C. M. Soukoulis, and S. Tretyakov, "Programmable metasurfaces: State of the art and prospects," in *IEEE Int. Sym. Circuits and Syst. (ISCAS)*, May 2018, pp. 1–5.
- [48] H. Yang, X. Cao, F. Yang, J. Gao, S. Xu, M. Li, X. Chen, Y. Zhao, Y. Zheng, and S. Li, "A programmable metasurface with dynamic polarization, scattering and focusing control," in *Scientific reports*, 2016.
- [49] M. Bloch, J. Barros, M. R. D. Rodrigues, and S. W. McLaughlin, "Wireless information-theoretic security," *IEEE Trans. Inf. Theory*, vol. 54, no. 6, pp. 2515–2534, Jun. 2008.
- [50] K. A. Hamdi, "Capacity of MRC on correlated Rician fading channels," *IEEE Trans. Commun.*, vol. 56, no. 5, pp. 708–711, May 2008.
- [51] J. Salo, H. M. El-Sallabi, and P. Vainikainen, "The distribution of the product of independent Rayleigh random variables," *IEEE Trans. Antennas Propag.*, vol. 54, no. 2, pp. 639–643, Feb. 2006.
- [52] S. Ross, *A First Course in Probability*, 7th ed. Pearson Education, Inc., New Jersey, 2006.